ACS Catalysis

Research Article

pubs.acs.org/acscatalysis

Pyridylamido Bi-Hafnium Olefin Polymerization Catalysis: Conformationally Supported Hf···Hf Enchainment Cooperativity

Yanshan Gao,[†] Aidan R. Mouat,[†] Alessandro Motta,[‡] Alceo Macchioni,*[,§] Cristiano Zuccaccia,*[,§] Massimiliano Delferro,*[,†] and Tobin J. Marks*[,†]

[†]Department of Chemistry, Northwestern University, Evanston, Illinois 60208, United States

[‡]Dipartimento di Scienze Chimiche, Università di Roma "La Sapienza" and INSTM, UdR Roma, piazzale Aldo Moro 5, I-00185 Roma, Italy

[§]Dipartimento di Chimica, Biologia e Biotecnologie and CIRCC, Università degli Studi di Perugia, Via Elce di Sotto, 8-06123 Perugia, Italy

Supporting Information

ABSTRACT: Homobimetallic Hf(IV) complexes, L^2-Hf_2Me_5 (**3**) and L^2-Hf_2Me_4 (**4**) (L^2 = *N*,*N*′-{[naphthalene-1,4-diylbis(pyridine-6,2-diyl)]bis[(2-isopropylphenyl)-methylene)]bis(2,6-diisopropylaniline}), were synthesized by reaction of the free ligand L^2 with the appropriate Hf precursor and were characterized in solution (NMR) and in the solid state (X-ray diffraction). In **3**, L^2 acts as a dianionic tridentate ligand for one Hf metal center and as a monoanionic bidentate ligand for the other, whereas in **4**, both Hf units are tricoordinated to opposite sides of L^2. In the solid state, the Hf···Hf distance is significantly different in **3** vs **4** (6.16 vs 8.06 Å, respectively), but in solution, the structural dynamics of the two linked metallic units in bis-activated complex **3** accesses conformers with far closer Hf···Hf distances (~3.2 Å). Once activated with $Ph_3C^+B(C_6F_5)_4^-$ (B_1) or $PhNMe_2H^+B(C_6F_5)_4^-$ (NB), **3** exhibits pronounced bimetallic cooperative effects in ethylene homopolymerization and ethylene +1-octene copolymerization vs the monometallic analogue L^1-$HfMe_2$ (**1**, L^1 = 2,6-diisopropyl-*N*-{(2-isopropylphenyl)[6-(naphthalen-1-yl)pyridin-2-yl]methyl}aniline) and bimetallic **4**, producing polyethylene with 5.7 times higher M_w and poly(ethylene-*co*-1-octene) with 2.4 times higher M_w and 1.9 times greater 1-octene enchainment densities than **1**. The activation chemistry of **3** and **4** with 1 or 2 equiv of B_1 and NB is characterized in detail by NMR spectroscopy. In sharp contrast to **1**, which undergoes Hf–C_{naph} protonolysis followed by naphthyl remetalation with NB as the cocatalyst, activation of **3** with B_1 or NB proceeds by consecutive $-CH_3$ protonolysis/abstractions at each Hf center, explaining the higher polymerization activity of **3**/NB versus **1**/NB. All product polymers have narrow (2–3) PDIs, and this is explained by NMR evidence for very fast exchange of alkyl moieties between the two active Hf metal centers. Key experimental findings are supported by DFT analysis.

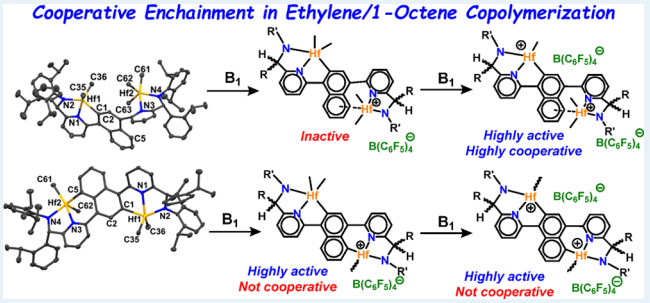

KEYWORDS: *hafnium, bimetallic, olefin polymerization, NMR spectroscopy, cooperativity effects*

1. INTRODUCTION

Multimetallic enzyme catalysts[1] achieve superior reactivity and selectivity via cooperative effects that often involve advantageous multiple active site–substrate interactions and proximities. As a conceptual inspiration, bimetallic strategies have been successfully applied in coordination polymerization catalysis, in which metal···metal cooperative effects dramatically impact catalytic behavior and product polymer microstructure.[2] In this regard, both homo- and heterobimetallic constrained geometry catalysts (Ti_2,[3] Zr_2,[4] Ti–Zr,[5] Ti–Cr;[6] Chart 1, A–B), and homobimetallic group 4[7] and group 10[8,9] phenoxyiminato catalysts (Chart 1, C–D) were shown to exhibit distinctive cooperative effects in producing polyolefins with substantially higher molecular weights (M_w's) and comonomer enchainment content versus the corresponding monometallic analogues. Although these phenomena have been explored for several organo-Ti and -Zr catalytic systems, little is known about the analogous Hf catalysts.[10] Indeed, hafnocene-based olefin polymerization catalysts have historically exhibited more sluggish polymerization activities while producing higher M_w polyolefins.[11] Beyond metallocenes, much recent progress has been made in the area of group 4 post-metallocene polymerization catalysts,[12] and this includes several unusual Hf-based systems. Thus, Sita and co-workers reported Hf catalyst **E** (Chart 2) capable of achieving living/coordinative chain-transfer polymerization (CCTP) of propylene in the presence of $ZnEt_2$ as a chain transfer agent (CTA).[10b,13] Active Hf catalysts based on bidentate [NN] ligands, such as **F**,[14] **G**,[15]

Received: April 15, 2015
Revised: July 25, 2015
Published: July 27, 2015

DOI: 10.1021/acscatal.5b00788
ACS Catal. 2015, 5, 5272–5282

Chart 1. Examples of Bimetallic Olefin Polymerization Catalysts

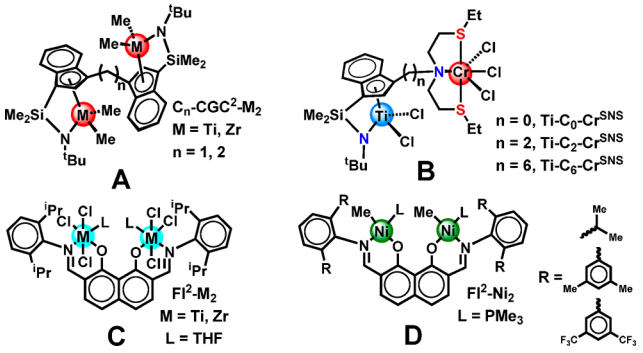

Chart 2. Representative Monometallic Hf Polymerization Catalysts

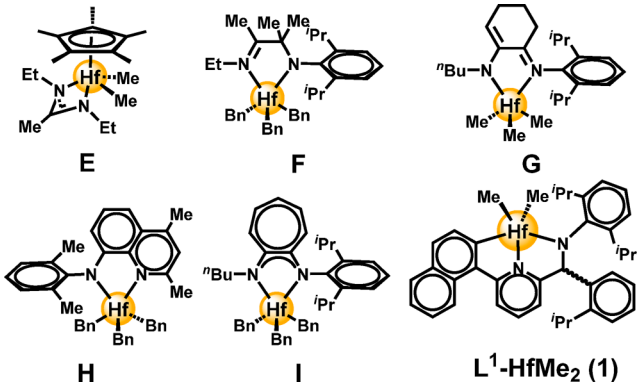

and **I**[16,17] (Chart 2), also exhibit high activity for olefin polymerization and copolymerization. However, some of these catalysts are thermally unstable and prone to ligand isomerization or addition processes. Compared with the corresponding Ti and Zr catalysts bearing the same ligands, the Hf catalysts generally exhibit far lower polymerization activity,[18] possibly reflecting increased monomer insertion barriers at Hf[19] or less efficient activation by MAO.[20]

A breakthrough in Hf-catalyzed olefin polymerization was reported by scientists at the Dow Chemical Co. and Symyx Technologies Inc. in 2003. They discovered a new Hf(IV) olefin (co)-polymerization catalyst (L^1-$HfMe_2$, **1**; L^1 = pyridylamido ligand, NNC type ligand) using high-throughput screening.[21] C_1-symmetric arylcyclo-metalated pyridylamido catalyst **1** (Chart 2) exhibits remarkable catalytic properties in producing high M_w, highly isotactic polypropylene in a high-temperature solution process.[22] Solution polymerizations at high temperatures avoid polymer precipitation; however, other homogeneous catalysts such as C_2-symmetric *ansa*-zirconocenes undergo thermal decomposition under these conditions.[23] Furthermore, catalyst **1** in tandem with a phenoxyiminato Zr catalyst and Et_2Zn affords olefin block copolymers having alternating semicrystalline and amorphous segments via catalytic ethylene/1-octene/$ZnEt_2$ "chain shuttling" polymerization (CSP).[2,24] Here, alkyl or polymeryl chains transfer between Hf (active for ethylene/1-octene copolymerization) and Zr (active for ethylene homopolymerization) catalytic centers via $ZnEt_2$. The drawback here is the requirement of large quantities of $ZnEt_2$ to ensure efficient polymeryl fragment shuttling between Hf and Zr centers.[24] Nevertheless, efficient CSP can be achieved via extensive high-throughput experimentation in flow reactors.[25]

When activated with $HNR_3^+B(C_6F_5)_4^-$ (R = alkyl), complex **1** produces ethylene/1-octene copolymers with high M_w (875 kg mol^{-1}) and a broad, bimodal PDI of 7.4.[22d,26] The broad PDI reflects an unusual activation process involving a single monomer insertion into the Hf–C_{naph} bond, yielding several ligand-modified active species.[22d] Moreover, the ~20 min induction period for catalyst **1**/$HNR_3^+B(C_6F_5)_4^-$ is attributed to initial protonolysis of the Hf–C_{naph} bond, followed by slow remetalation to afford the cationic precursor of the active catalyst.[22c] Considering the importance of Hf-based olefin polymerization catalysis both in industry and academia, it is tempting to design bimetallic Hf complexes for cooperative olefin polymerization catalysis. Bimetallic and monometallic comparisons should provide more detailed understanding of the unusual activation chemistry and cooperative/intramolecular processes in pyridylamido Hf polymerization catalysis.

Here, we report the synthesis, characterization, and olefin polymerization characteristics of the bimetallic pyridylamido Hf complexes shown in Chart 3. It will be seen that when activated

Chart 3. Structures of the Present Pyridylamido Hf Complexes

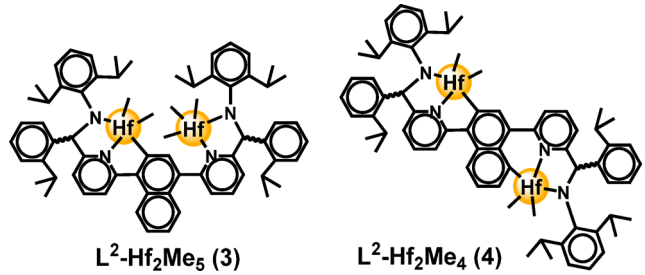

with 2 equiv of cocatalyst $Ph_3C^+B(C_6F_5)_4^-$ (B_1) or $HNR_3^+B(C_6F_5)_4^-$ (NB), catalyst **3** affords polymers with significantly higher comonomer incorporation and higher M_w in comparison with monometallic catalyst **1** and bimetallic **4** with less proximate Hf centers. Thus, bimetallic cooperative effects are strongly influenced by Hf center spatial proximity, with bis-activated **3** having a Hf···Hf distance of 3.2–6.6 Å (see computed structural dynamics in the Supporting Information) affording substantial cooperative enchainment effects. On the other hand, bis-activated **4** with similar ligation but with a fixed Hf···Hf distance of 7.5 Å affords negligible effects. All product polymers are monomodal with narrow PDIs (2–3), characteristic of well-defined single-site behavior. Solution phase NMR spectroscopic and DFT probes of the structure–reactivity properties of the dicationic catalysts provide a molecular level picture of the distinctive bimetallic chemistry. Different activation pathways, identified by NMR, convincingly explain the differing induction periods observed for **3**/NB and **1**/NB, whereas VT ^{1}H ROESY NMR, supported by DFT computation, argues that fast intramolecular exchange/chain shuttling of alkyl moieties between Hf centers is possible under catalytic conditions.

2. RESULTS

The goal of this investigation is to explore and understand possible cooperative olefin enchainment effects in a family of bimetallic Hf pyridylamido catalysts, focusing on unusual ethylene polymerization and ethylene + α-olefin copolymeriza-

DOI: 10.1021/acscatal.5b00788
ACS Catal. 2015, 5, 5272–5282

tion behavior. Specifically, (1) the synthesis, solid state and solution structural, and cocatalytic activation chemistry of bimetallic complexes **3** and **4** are described; (2) their implementation in ethylene homopolymerization and ethylene/1-octene copolymerization are compared and contrasted with mononuclear catalyst **1**, revealing pronounced, distance dependent bimetallic Hf···Hf effects on polymerization activity, product M_w, and selectivity for 1-octene enchainment; (3) comparative polymerization experiments using 1.0 and 2.0 equiv of cocatalyst are explored to clarify cooperative effects; (4) the activation chemistry of the bimetallic complexes with B_1 or NB are compared using a variety of NMR techniques; (5) the origin of the bimetallic cooperative effects in this Hf pyridylamido series are further clarified by DFT techniques.

2.1. Synthesis of Pyridylamido Ligand L^2. The synthesis of ligand L^2 is shown in Scheme 1. Suzuki coupling of bromopyridyl imine intermediate **I** and naphthalene-1,4-diboronic acid **II** provides naphthalene-1,4-dipyridyl imine intermediate **III**. Bimetallic ligand (L^2) is then prepared by nucleophilic addition of in situ-generated 2-isopropylphenyl lithium to the imine intermediate **III**. The reaction proceeds in good-to-high yield and affords ligand L^2 in high purity, as confirmed by conventional spectroscopic and analytical techniques. For comparison, ligand L^1 and the corresponding monometallic complex **1** are also synthesized according to the literature.[26]

Scheme 1. Synthesis of Binuclear Pyridylamido Ligand L^2

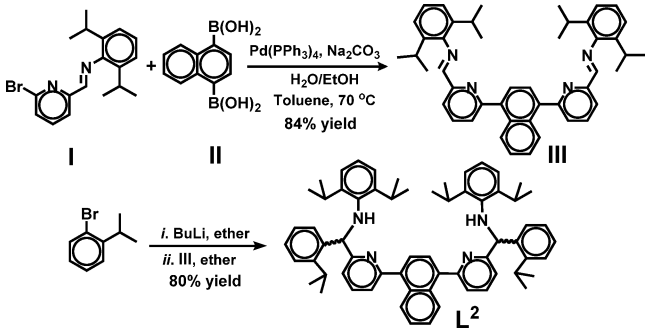

2.2. Synthesis and Characterization of Bimetallic Pyridylamido Hf Complexes. *2.2.1. Synthesis of Bimetallic Hf-Methyl Complex* ***3****.* Complex **3** was synthesized by overnight alkylation of the corresponding Hf amido complex **2**[27] with trimethylaluminum in toluene at 25 °C (Scheme 2). An alternative route to **3** is by metalation of ligand L^2 with *n*-BuLi followed by reaction with $HfCl_4$ at 110 °C. Subsequent overnight reaction with CH_3MgBr at 25 °C affords complex **3**. Single crystals of **3** suitable for X-ray diffraction were obtained by slow evaporation of a pentane/ether solution (Figure 1A).

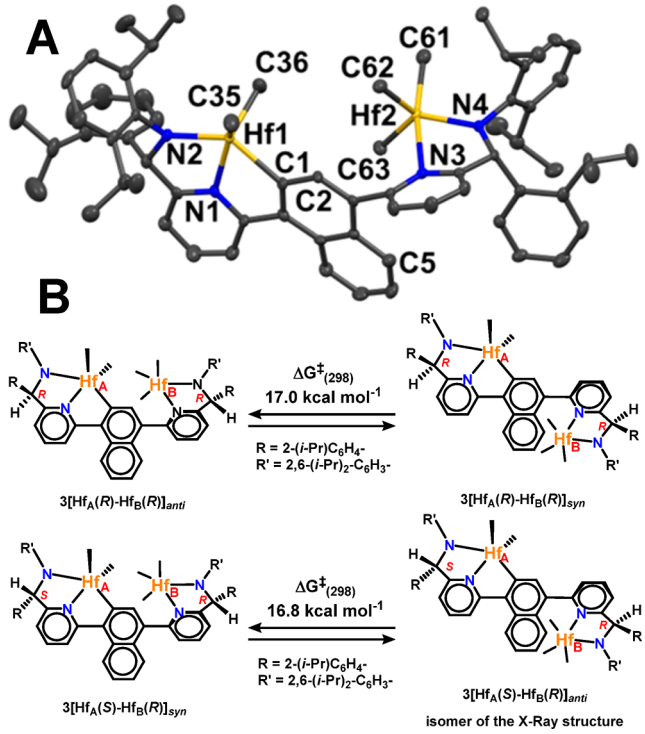

Figure 1. (A) ORTEP plot of complex $3[Hf_A(S)–Hf_B(R)]_{anti}$. Thermal ellipsoids are drawn at the 30% probability level. H atoms are omitted for clarity. (B) Rotamer interconversions identified in $3[Hf_A(R)–Hf_B(R)]_{syn/anti}$ and $3[Hf_A(S)–Hf_B(R)]_{syn/anti}$; here, syn and anti refer to the relative position of the $HfMe_3$ and C–H of the chiral bridge closest to Hf_A with respect to the average plane defined by the naphthyl ring.

Both Hf centers adopt distorted trigonal bipyramidal geometries with an intramolecular Hf···Hf distance of 6.16 Å. The $HfMe_2$ center is almost coplanar with the naphthalene plane (dihedral angle = 7.9°), and the $HfMe_3$ group is nearly perpendicular to the naphthalene plane (dihedral angle = 102.8°). This twisted structure likely minimizes unfavorable steric repulsions.

Methylation of complex **2** affords 5-membered Hf_2 metallacycle **3** with metalation on only one side of the molecule

Scheme 2. Synthesis of Bimetallic Pyridylamido Hf Complex L^2-Hf_2Me_5 (3)

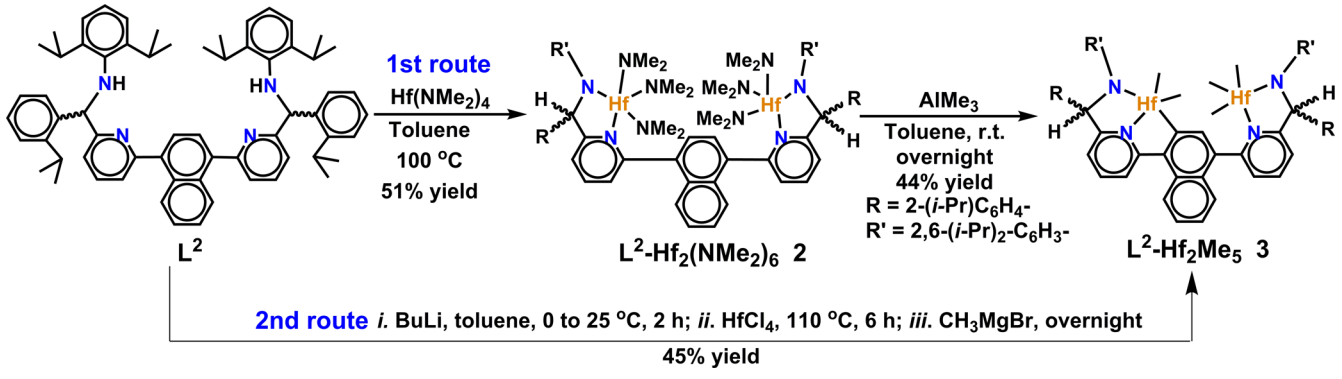

DOI: 10.1021/acscatal.5b00788
ACS Catal. 2015, 5, 5272–5282

(Scheme 2). A second C−H_{naph} activation to produce another 5-membered metallacycle is apparently unfavorable for steric reasons. The NMR data indicate that complex **3** is present in solution as a mixture of isomers (see Figure S5) and show, in agreement with the X-ray findings, that aryl cyclometalation occurs only on one side of the L^2 ligand. Indeed, all the high-frequency ^{13}C NMR resonances (δ_C = 208.2, 205.1, 203.2, and 201.9 ppm) have long-range ^1H, ^{13}C scalar correlations with the corresponding H2 resonances, indicating that metalation is C1-selective in all isomers. Four isomers account for ∼80% of the mixture. On the basis of detailed ^1H NOESY NMR analysis, which reveals a selective chemical exchange process between pairs of isomers (Figure 1B), we propose that in solution, **3** is present largely as a mixture of diastereomers, **3**$[Hf_A(S)-Hf_B(R)]_{syn/anti}$ and **3**$[Hf_A(R)-Hf_B(R)]_{syn/anti}$, each of which is equilibrating between two limiting rotamers arising from the rotation of the entire $HfMe_3$ unit around the $C_{naph}-C_{Py}$ linkage (Figure 1). The diastereomer molar ratio is ∼55/45, and the relative abundance of the two rotamers is ∼65/35 for both diastereomers. The interconversion barrier between rotamers was evaluated by VT ^1H EXSY NMR (278−298 K) in toluene-d_8, affording $\Delta G^{\ddagger}_{(298)} \approx 16.9 \pm 1.0$ kcal mol^{-1} for both diastereoisomers (Table S1). Such a value is ∼1.7 kcal mol^{-1} lower than that associated with an approximate 180° rotation of the 2-(*i*-Pr)C_6H_4 units about the C−C bond.[26,28] From the thermodynamic viewpoint, the latter equilibration likely explains the presence of additional species (∼20%) in the mixture.[26,28]

2.2.2. Synthesis of Bimetallic Hf−Methyl Complex 4. When complex **3** is heated in toluene at 90 °C for 2 h, the ^1H NMR spectrum shows the disappearance of **3** with formation of new sets of resonances assignable to complex L^2-Hf_2Me_4 (**4**) and 1.0 equiv of CH_4 (Scheme 3). Complex **4** is mainly present in

Scheme 3. Synthesis of Bimetallic Complex L^2-Hf_2Me_4 (4)[a]

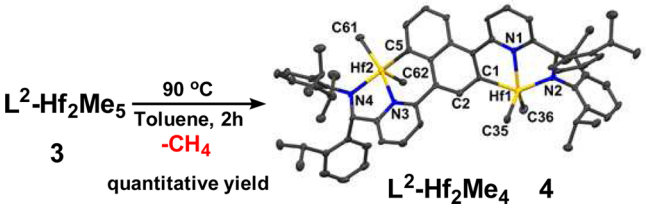

[a]ORTEP thermal ellipsoids are drawn at the 30% probability level. H atoms and solvent molecules are omitted for clarity.

solution as a mixture of two diastereomers in a ∼57/43 molar ratio (see Figure S9). The key NMR fingerprint of **4** is the presence of two high-frequency ^{13}C NMR resonances for the aryl-metalated carbon atoms of each diastereomer. Specifically, two signals (δ_C = 202.0 and 203.7 ppm) give long-range correlations with the singlets of H2 in the 5-membered metallacycle at δ_H = 9.10 and 9.13 ppm, and are attributed to C1 of the major and minor diastereomers, respectively. The other two signals (δ_C = 206.3 and 206.4 ppm) show long-range correlation with the doublets assigned to H6 of the 6-membered metallacycle at δ_H = 8.89 and 8.86 ppm, and are assigned to C5 resonance of the major and minor diastereomer, respectively (see Figure S9). These data indicate that **4** is obtained from **3** as a consequence of a second C−H_{naph} activation at C5 with concomitant CH_4 elimination.

The molecular structure of **4** was determined by X-ray diffraction studies of single crystals grown from toluene/pentane solutions. An ORTEP drawing shown in Scheme 3 reveals that Hf1 has a 5-coordinate, distorted trigonal bipyramidal geometry with the ligand skeleton distorted from an ideal plane by a twist angle of 10.3(4)°. The C1−Hf1−N2 bond angle is 140.9(3)°, indicating severe distortion from the ideal 180°, with the Hf displaced toward the methyl groups, most likely a result of steric repulsion. The C35−Hf1−C36 bond angle is 108.0(4)°, less than the ideal 120°, and the C36−Hf1−N1 bond angle is 134.4(3)°, evidencing marked structural distortion. The Hf2 center has a 5-coordinate distorted square pyramidal geometry with the Hf displaced 0.625(4) Å from the plane defined by the basal ligands toward the apical methyl group. Within the basal plane, the C5−Hf2−C61 bond angle is 96.9(3)°; the C61−Hf2−N4 bond angle is 95.8(3)°, the C5−Hf2−N3 bond angle is 79.4(3)°, and the N3−Hf2−N4 bond angle is 72.6(2)°, indicating a splaying of the methyl groups induced by the narrower chelating backbone bite angle. The C61−Hf2−C62 bond angle is 105.8(3)°, strongly distorted from the ideal 90°, and is consistent with the significant displacement seen in the Hf center. The Hf···Hf distance in **4** is 8.060(3) Å.

2.3. Olefin Polymerization Studies. Initial ethylene polymerization experiments were carried out with bimetallic catalyst **3** in the presence of B_1 ($Ph_3C^+B(C_6F_5)_4^-$) or NB ($PhNMe_2H^+B(C_6F_5)_4^-$) as the cocatalyst/activator under rigorously anhydrous/anaerobic conditions to find the optimum polymerization conditions (temperature, pressure, an time). Exothermic and mass transfer effects were minimized by very rapid stirring.[9a,29] At different temperatures (40, 60, 80, and 100 °C) under constant 1 atm ethylene pressure, the highest activities were achieved at 60 and 80 °C, and higher temperatures (100 °C) led to catalyst deactivation. Higher ethylene pressures (3, 5 atm) or longer reaction times (5 min) were also examined; however, under these conditions, the precipitation of the polymer interferes with stirring and temperature control. Thus, the overall optimum catalytic performance (activity, M_w, PDI, cooperative effects) is achieved at 80 °C under constant ethylene pressure of 1.0 atm for 1 min. The data in Table 1 show that all polymer products are monomodal with PDIs consistent with single-site processes.[30]

2.3.1. Ethylene Homopolymerization Catalysis with 2 Equiv of Activator. Bimetallic catalyst **3** activated with B_1 yields ∼5.7 times higher M_w polyethylene product than that of the monometallic catalyst **1** (with 1 equiv activator), but with ∼3.7

Table 1. Ethylene Homolymerization Data.[a]

entry	cat. (μmol)	cocat. (μmol)	PE (g)	act.[b]	M_w[c]	PDI[c]	active species[d]
1	**1** (10)	B_1 (12)	1.020	102.0	245	2.3	
2	**3** (5)	B_1 (12)	0.276	27.6	1387	3.4	**6**
3	**3** (10)	B_1 (10)	0.064	3.2	179	2.4	**5**
4	**4** (5)	B_1 (12)	0.410	41.0	259	2.8	**9**
5	**4** (10)	B_1 (10)	0.516	25.8	186	2.4	**8**
6	**1** (10)	NB (12)	0.022	2.2	234	2.3	
7	**3** (5)	NB (12)	0.230	23.0	386	2.5	**7**
8	**3** (10)	NB (10)	0.141	7.1	148	2.5	**5**
9	**4** (5)	NB (12)	0.266	26.6	281	2.4	**7**
10	**4** (10)	NB (10)	0.315	15.8	123	2.8	**5** (7)[32]

[a]Conditions: B_1 = $Ph_3C^+B(C_6F_5)_4^-$; NB = $PhNMe_2H^+B(C_6F_5)_4^-$; $P_{ethylene}$ = 1 atm; toluene = 50 mL; 80 °C; time, 1 min. Each entry was performed in duplicate. [b]Units: (kg of polymer)·(mol of Hf)$^{-1}$ min^{-1} atm^{-1}. [c]GPC versus polystyrene standards in (kg·mol^{-1}). [d]By NMR.

DOI: 10.1021/acscatal.5b00788
ACS Catal. 2015, 5, 5272−5282

Table 2. Ethylene/1-Octene Co-Polymerization Data.[a]

entry	cat. (μmol)	cocat. (μmol)	poly. (g)	act.[b]	M_w[c]	PDI[c]	inc.[d]	active species[f]
1	**1** (10)	B_1 (12)	1.591	159.1	355	1.8	14.9	
2[e]	**1** (10)	B_1 (12)	2.720	272.0	240	2.1	34.2	
3	**3** (5)	B_1 (12)	0.649	64.9	862	3.1	28.7	**6**
4[e]	**3** (5)	B_1 (12)	1.519	151.9	360	2.2	60.5	**6**
5	**3** (10)	B_1 (10)	trace					**5**
6	**4** (5)	B_1 (12)	1.128	112.8	174	2.7	18.6	**9**
7	**4** (10)	B_1 (10)	1.132	56.6	265	2.7	20.3	**8**
8	**1** (10)	NB (12)	0.042	4.2	218	2.3	11.7	
9	**3** (5)	NB (12)	0.613	61.3	409	2.4	18.0	**7**
10	**3** (10)	NB (10)	0.066	3.3	235	3.0	6.8	**5**
11	**4** (5)	NB (12)	0.684	68.4	1181	3.3	17.0	**7**
12	**4** (10)	NB (10)	0.461	23.1	266	2.6	13.0	**5** (7)[20]

[a]Conditions: B_1 = $Ph_3C^+B(C_6F_5)_4^-$; NB = $PhNMe_2H^+B(C_6F_5)_4^-$; $P_{ethylene}$ = 1 atm; [1-octene] = 0.72 g; toluene = 50 mL; 80 °C; time, 1 min. Each entry was performed in duplicate. [b]Units (kg polymer)·(mol of Hf)$^{-1}$ min^{-1} atm^{-1}. [c]GPC versus polystyrene standards in (kg·mol^{-1}). [d]Mol % 1-octene incorporation, assayed by ^{13}C NMR.[34] [e][1-Octene] = 2.15 g. [f]By NMR.

times lower activity (Table 1, entries 1 and 2). This fall in activity probably reflects steric constraints.[31] Interestingly, complex **4** exhibits activity similar to that of bimetallic **3** and produces PE with a M_w comparable to that obtained with monometallic complex **1** (Table 1, entry 3), suggesting that the activity is affected by steric hindrance around the metal centers and no significant cooperative effects are operative in bimetallic catalyst **4**. However, when NB is used as the cocatalyst, **3** attains ∼10.7 times higher activity and slightly higher M_w than monometallic **1** (Table 1, entries 6 and. 7). The lower activity of **1** may reflect the requirements of an induction period,[22c] whereas the bimetallic catalyst **3** appears to be active immediately. ^{13}C NMR analysis of the PEs produced by catalysts **1**, **3**, and **4** activated with either B_1 or NB indicate highly linear structures with no detectable branching.

2.3.2. Control Experiments: Ethylene Homopolymerization with 1 Equiv of Activator. Activation with 1 equiv of B_1 or NB yields rather different results for **3** vs **4**. For complex **3**, a dramatic fall in activity, from 27.6 to 3.2 (kg polymer)·(mol of Hf)$^{-1}$ min^{-1} atm^{-1} for B_1 and from 23.0 to 7.1 (kg polymer)·(mol of Hf)$^{-1}$ min^{-1} atm^{-1} for NB is observed, and polymer M_w falls from 1387 to 179 kg mol^{-1} for B_1 and from 386 to 148 kg mol^{-1} for NB (Table 1, entries 2 vs 3, 7 vs 8). Note that this decrease in M_w suggests that the enchainment process catalyzed by bimetallic complex **3** is likely governed by cooperative rather than steric effects, insofar as the two active species **5** and **6** have similar steric characteristics around the metal centers (vide infra). In contrast, for bimetallic complex **4** under the same conditions, there is only a 1.6 times decrease in activity (from 41.0 to 25.8 (kg polymer) (mol of Hf)$^{-1}$ min^{-1} atm^{-1}) and marginal changes in polymer M_w (from 259 to 186 kg mol^{-1};Table 1, entries 4 vs 5). Here, performance is only marginally activator-stoichiometry- and identity-sensitive, arguing that neither cooperative nor differential ion-pairing effects dominate.

2.3.3. Ethylene/1-Octene Copolymerization with 2 Equiv of Activator. In ethylene/1-octene copolymerizations, bimetallic complex **3** activated with B_1 exhibits greater 1-octene incorporation (28.7 vs 14.9 mol %), generates higher M_w's (862 vs 355 kg mol^{-1}), with slightly broader PDIs (3.1 vs 1.8), than monometallic control **1** (with 1 equiv of activator; Table 2, entries 3 vs 1). In marked contrast, bimetallic complex **4** yields 1-octene incorporation levels (18.6 mol %) very similar to the monometallic control **1**, and with a lower product M_w (174 kg mol^{-1}, Table 2, entry 6), arguing that the two metal centers in bimetallic complex **4** operate independently. These results and those in the section above likely reflect the nonideal spatial conformations and large catalytic center separation in **4** vs **3**. Curiously, with NB as the cocatalyst, complexes **3** and **4** exhibit similar copolymerization properties, that is, activity, 61.3 (kg polymer)·(mol of Hf)$^{-1}$ min^{-1} atm^{-1} for **3** and 68.4 (kg polymer)·(mol of Hf)$^{-1}$ min^{-1} atm^{-1} for **4**; 1-octene incorporation, 18.0 mol % for **3** and 17.0 mol % for **4** (Table 2, entries 9 and 11), indicating that both activators generate functionally similar active species with NB (vide infra). In surprising contrast, mononuclear complex **1** (with 1 equiv of NB; Table 2, entry 8) under the same polymerization conditions exhibits near-negligible activity (4.2 (kg polymer)·(mol of Hf)$^{-1}$ min^{-1} atm^{-1}), ∼16 times less than those of **3** and **4**, presumably reflecting the aforementioned slow remetalation process,[22c] and slightly lower comonomer incorporation (11.7 mol %), ∼1.5 times less than those of **3** and **4**. When higher 1-octene concentrations are introduced in copolymerization (from 0.72 to 2.15 g) experiments, bimetallic catalyst **3**/B_1 enchains 26.3 mol % more 1-octene and yields higher M_w polymers than does monometallic catalyst **1**/B_1 (60.5 vs 34.2 mol %, 360 vs 240 kg mol^{-1}, Table 2, entries 4 and 2, respectively). Note also that ethylene/1-octene copolymerization activities are greater than those for ethylene homopolymerization, a not uncommon comonomer rate enhancement effect.[33]

Ethylene + 1-octene reactivity ratio estimations were made using ^{13}C NMR methods (Table S3) for a single concentration of α-olefin ([1-octene] = 0.72 g).[35] Although bimetallic catalyst **3**/2B_1 shows a higher 1-octene incorporation ratio than **1**/1B_1 (Table 2, entries 3 vs 1), its reactivity ratio for 1-octene ($r_{1\text{-octene}}$ = 0.44) is less than that of the monometallic control **1**/1B_1 ($r_{1\text{-octene}}$ = 0.77). In contrast, the monometallic catalyst exhibits a much larger $r_{ethylene}$ (11.80 vs 3.43). The product of monomer reactivity ratios ($r_{ethylene}r_{1\text{-octene}}$) indicates that the poly(ethylene-*co*-1-octene) produced by bimetallic **3** is close to a statistically random copolymer ($r_{ethylene}r_{1\text{-octene}}$ = 1.50),[36] whereas the polymer produced by monometallic catalyst **1** has significant block alternating [EEE]−[OOO] character ($r_{ethylene}r_{1\text{-octene}}$ = 9.08).[36] Note also that the polymer microstructures are not affected by the different cocatalysts, insofar as $r_{ethylene}r_{1\text{-octene}}$ does not change significantly using B_1 or NB. These observations suggest that the catalytic centers in

DOI: 10.1021/acscatal.5b00788
ACS Catal. 2015, 5, 5272−5282

Scheme 4. Activation Chemistry of Bimetallic Complexes 3 and 4 According to NMR Analysis

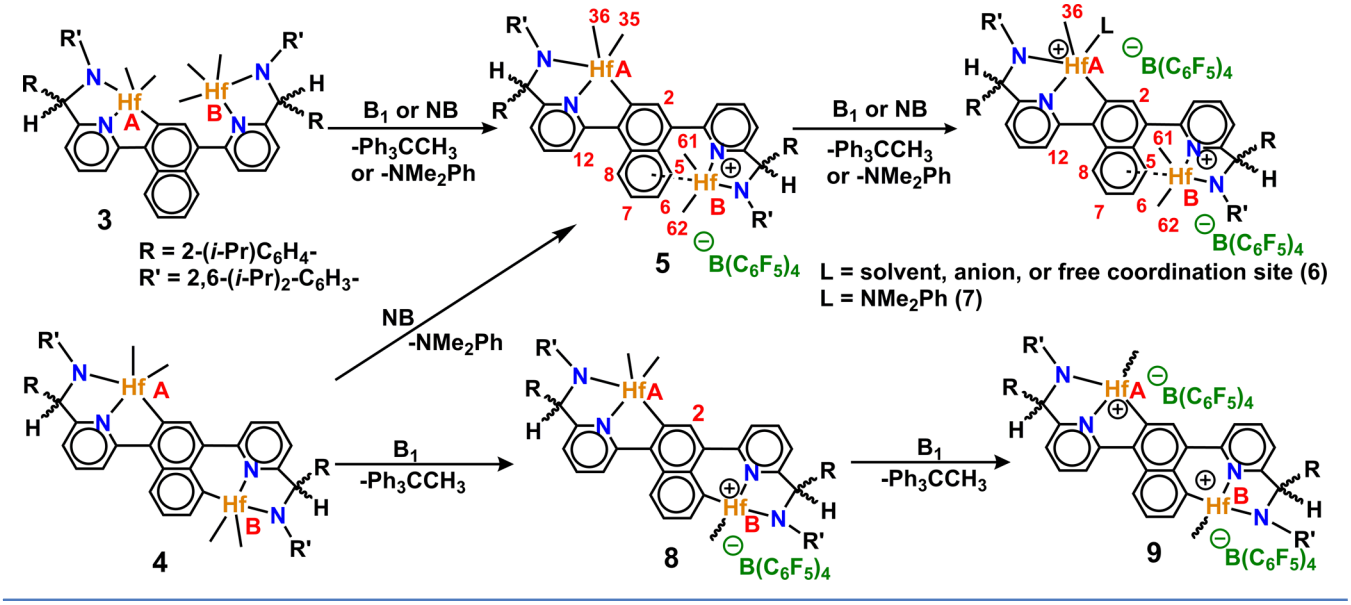

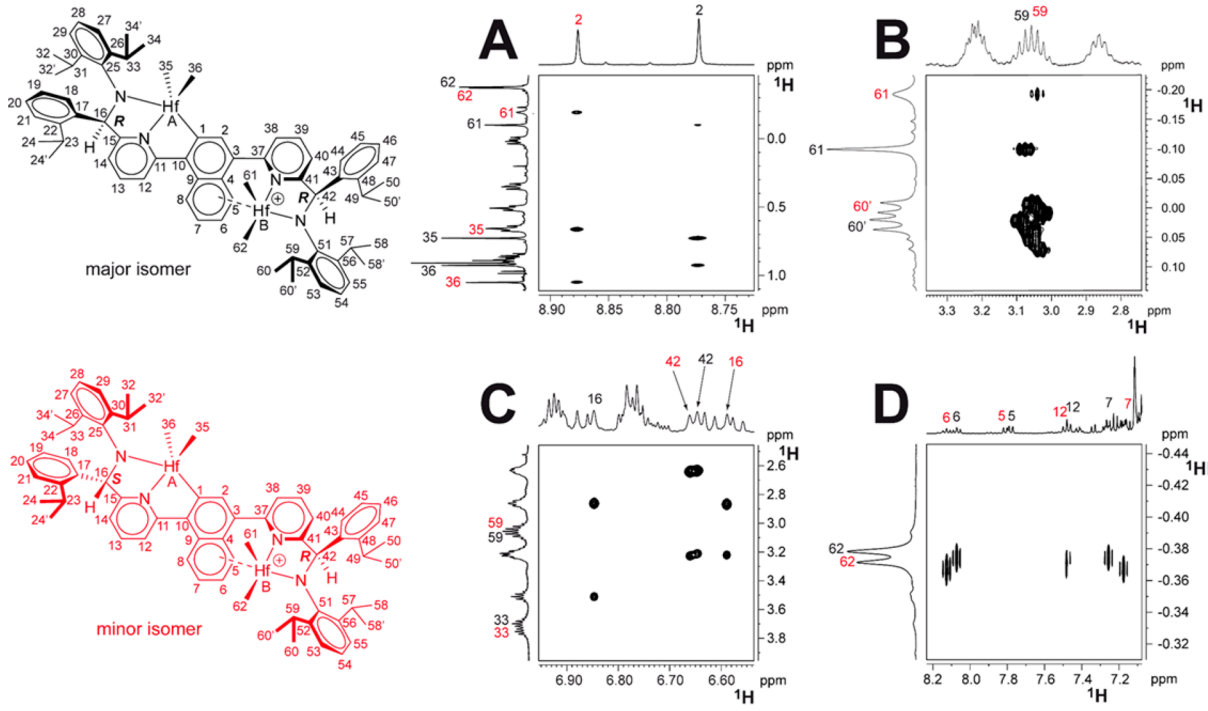

Figure 2. Four sections of the ^{1}H ROESY NMR spectrum of ion pair **5** (toluene-d_8, 268 K). Black and red colors refer to the **5**[$Hf_A(R)$–$Hf_B(R)$] and **5**[$Hf_A(S)$–$Hf_B(R)$] diastereomers, respectively.

bimetallic active species **6** and **7** are more sterically congested than the monometallic analogue. Steric constraints probably render consecutive 1-octene enchainment at the Hf–C (polymeryl) bond less favorable for bimetallic **3**, despite the higher 1-octene incorporation tendency vs the monometallic analogue.

2.3.4. Control Experiments: Ethylene/1-Octene Copolymerization with 1 Equiv of Activator. When the loadings of cocatalysts B_1 and NB are decreased from 2 to 1 equiv with respect to catalyst metal centers, only trace polymer is obtained from complex **3** (Table 2, entries 5 and 10); however, no obvious change in polymer yield, polymer M_w, and 1-octene incorporation level is observed for bimetallic **4** (Table 2, entries 7 vs 12).

2.4. Catalyst Activation Chemistry. The activation chemistry of **3** and **4** with typical Lewis (B_1) or Brønsted (NB) acid cocatalysts was investigated in solution by advanced NMR methods[37] using 1 or 2 equiv of cocatalyst/metal center (Scheme 4).

2.4.1. Bimetallic Complex 3. The reaction of complex **3** with 1 equiv of B_1 or NB proceeds in a similar manner, affording, after abstraction/protonolysis of a single methyl group from the $HfMe_3$ unit, monocationic complex **5** (Scheme 4). In solution **5** is present predominantly as a mixture of two diastereomers in a ~55/45 molar ratio. NMR resonance assignment was carried

DOI: 10.1021/acscatal.5b00788
ACS Catal. 2015, 5, 5272–5282

out starting from H2 (s, δ_H = 8.77 ppm for the major isomer; δ_H = 8.87 ppm for the minor isomer) and following both dipolar and scalar interactions in 2D homo- and heteronuclear NMR experiments (relevant sections of the ^{1}H ROESY NMR spectrum are shown in Figure 2). The negative chemical shift values of H61 and H62, the NOE contacts of H62 with H6 and H7 (Figure 2D), and the low value of the C5 chemical shift (δ_C = 114.9 ppm for the major isomer, δ_C = 114.7 ppm for the minor isomer) all indicate π-coordination of the naphthyl to Hf_B, as previously observed, both in solution and in the solid state, for the monometallic ion-paired analogue, L^1-$HfMe_2^+$B-$(C_6F_5)_4^-$, obtained from reaction of **1** with NB.[22c] Furthermore, an NOE contact between H61 and the septet at δ_H = 3.04 ppm (H59) is also present (Figure 2B), whereas the latter septet does not show significant NOE with H42 (Figure 2C). This indicates that H61 is *anti* with respect to H42, leading to the conclusion that the configuration of the two chiral carbon atoms of the major diastereomers is **5**[Hf_A(*R*)−Hf_B(*R*)] or its enantiomer **5**[Hf_A(*S*)−Hf_B(*S*)]. Consequently, the configuration of the two chiral carbons of the minor diastereomer is **5**[Hf_A(*S*)−Hf_B(*R*)] or its enantiomer **5**[Hf_A(*R*)−Hf_B(*S*)].

The activation of **3** with 2 equiv of B_1 or NB produces dicationic complex **6** or the corresponding aniline−stabilized complex **7**, respectively (Scheme 4). The low frequency shifts of H61, H62, and C5, as well as the NOE contacts of H62 with H6 and H7 in both **6** and **7** (see for example Figure S18) indicate that the structure around Hf_B is similar to that in **5**. Consequently, the second equiv of cocatalyst selectively abstracts/protonate one methyl group from the Hf_A unit, with concomitant aniline coordination to Hf_A in the case of **7**.[38] This is in sharp contrast to the behavior of **1**, which undergoes selective protonolysis of Hf−C_{naph} σ-bond when activated with NB.[22d] Possibly the presence of the cationic Hf_B unit, already involved in π-coordination with the naphthyl moiety (i.e., **5**), favors selective protonolysis of Hf−C_{Me} σ-bond at the Hf_A site, providing a rationale for the high activity and lack of induction period in polymerizations mediated by **3**/2 NB (vide supra).

A common and interesting feature of ion pairs **5** and **6** is the presence of a dynamic process that selectively exchanges CH_3 groups between Hf_A and Hf_B centers. In particular, Me(36)−Me(61) exchange is operative in **5**[Hf_A(*R*)−Hf_B(*R*)] and **6**, whereas Me(35)−Me(61) exchange is operative in **5**[Hf_A(*S*)−Hf_B(*R*)] (see the SI). Variable-temperature ^{1}H EXSY NMR studies in toluene-d_8, (228−288 K, see the SI) yield $\Delta G^{\ddagger}_{(298)}$ = 15.5 ± 1.0 and 14.3 ± 1.0 kcal mol^{-1} for methyl group exchange in **5**[Hf_A(*R*)−Hf_B(*R*)] and **5**[Hf_A(*S*)−Hf_B(*R*)], respectively. These values compare well with those recently measured for methyl exchange in the heterobimetallic adduct formed by **1**$^+$B$(C_6F_5)_4^-$ and $ZnMe_2$ ($\Delta G^{\ddagger}_{(298)}$ = 14−16 kcal mol^{-1}).[22f] The corresponding ethyl exchange rate in the heterobimetallic adduct formed by **1**$^+$B$(C_6F_5)_4^-$ and $ZnEt_2$ also occurs at a similar (if not larger) rate.[22f] Consequently, the fast methyl exchange observed in **5** and **6** suggests that alkyl groups can rapidly and reversibly transfer between the Hf_A and Hf_B catalytic centers in the present binuclear systems, as also suggested by DFT calculations (vide infra). The aforementioned exchange process is not operative in **7** at room temperature, presumably because of aniline coordination.

2.4.2. Bimetallic Complex 4. The reaction of **4** with 1 equiv of NB proceeds by the selective protonation at C5, affording **5** (Scheme 4). In contrast, complex **4** reacts with 1 equiv of B_1 to form a complex mixture containing four major species. Interestingly, the ^{1}H ROESY NMR spectrum establishes that in all four species, the H2 resonance gives NOE contacts with two singlets in the aliphatic region arising from Hf−CH_3 moieties, confirmed by an ^{1}H, ^{13}C HMQC experiment (Figure S22). It thus appears that B_1 regioselectively abstracts one CH_3 group from the Hf_B unit of **4**, affording monocationic complex **8**. Formation of four different species can be explained by considering that the abstraction of one CH_3 from Hf_B may not be stereoselective (see Scheme S7) as observed when **1** is activated with B_1.[22c] The reaction of **4** with 2 equiv of B_1 yields a complex mixture. In contrast to that found for **8**, the ^{1}H ROESY NMR experiment establishes that, for each of the three principal species, the H2 resonance gives NOE contacts with only one singlet in the aliphatic region that is assigned to the corresponding Hf_A−CH_3 moieties, as confirmed by a ^{1}H, ^{13}C HMQC NMR experiment (Figure S24). Consequently, the second equiv of B_1 regioselectively abstracts one CH_3 group from the Hf_A unit of **8**, affording a diastereomeric mixture of dicationic complex **9** (Scheme 4).

2.5. DFT Analysis. DFT calculations were performed to obtain further insight into the structural and electronic properties of the catalytically active species and to explain the unusual catalytic behavior of the two bimetallic systems versus the monometallic analogue. First, geometrical analysis of dicationic complex **6**, obtained by the activation of **3** with cocatalyst B_1 and the corresponding aniline-stabilized complex **7**, obtained by the activation of **3** with cocatalyst NB, are performed. Only diastereomer, *R*,*R* was analyzed. Three main configurations found for dicationic complex **6** are related by rotation of the Hf_BMe_2 unit around the C_{naph}−C_{Pyr} bond. The most stable structure (the other structures are depicted in Figure S72) features two μ-CH_3 groups bridging the Hf sites (Figure 3A). This configuration involves elongation of the Hf−CH_3 bonds as well as reorientation of the CH_3 groups involved in the bridge. The isopropyl fragment of the 2-(*i*-Pr)C_6H_4− moiety points far away from the metal center at both Hf_A and

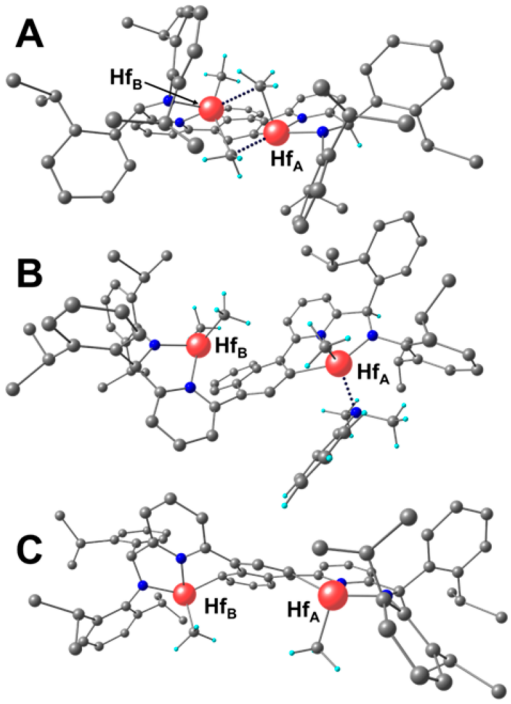

Figure 3. DFT optimized structures of dicationic complexes **6** (A), **7** (B), and **9** (C).

DOI: 10.1021/acscatal.5b00788
ACS Catal. 2015, 5, 5272−5282

Hf_B sites. Overall, the computed Hf···Hf distance in complex **6** lies in the 3.20−6.55 Å range, depending on the rotational conformation of the Hf_BMe_2 unit around the C_{naph}−C_{Pyr} bond. For dicationic complex **7**, the Hf_BMe_2 unit and the C−H of the chiral bridge proximate to Hf_A are in an *anti* position with respect to the naphthalene plane (Figure 3B), whereas a *syn* arrangement is found between the Hf_BMe_2 unit and the CH_3 group bonded to the Hf_A site. Here, the isopropyl fragment of the 2-(*i*-Pr)C_6H_4− moiety is directed toward the metal center in the Hf_A site and far away from the metal center in the Hf_B site.

The different fragment arrangements of complex **6** vs **7** reflect the aniline coordination to the Hf_A site. Note also that any attempt to force coordination of aniline to the Hf_B site destabilizes the structures by ∼24 kcal/mol. In contrast, similar aniline coordination to the activated catalyst arising from parent monometallic catalyst **1** yields a more stable complex by ∼5 kcal/mol vs coordination of the aniline to the Hf_A site in complex **7**. Finally, dicationic complex **9** (Figure 3C) arising from the activation of catalyst **4** with B_1 has both Hf sites fused to the naphthyl ring in a rigid conformation. In contrast to **6**, the long Hf···Hf distance in **9** is fixed at 7.48 Å.

3. DISCUSSION

Evidence from the DFT calculations,[29] NMR analysis,[22b] and extensive polymerization experiments[22a,b] as well as catalytic data from similar systems[28,39] persuasively argues that a monoalkyl cationic Hf(IV) center having a Hf−C_{naph} σ-bond is essential for achieving high polymerization activity in monometallic Hf arylcyclometalated pyridylamido catalysts. These requirements appear to hinge on the in situ generation of a remarkably active species via a single olefin molecule insertion into the Hf−C_{naph} σ-bond. This is facile when a CH_3 abstractor such as B_1 is used as the cocatalyst (Scheme 5, top). In contrast,

Scheme 5. Initial Migratory Insertion of Ethylene into the Hf−C_{naph} Bond of Monometallic Pyridylamido Complexes

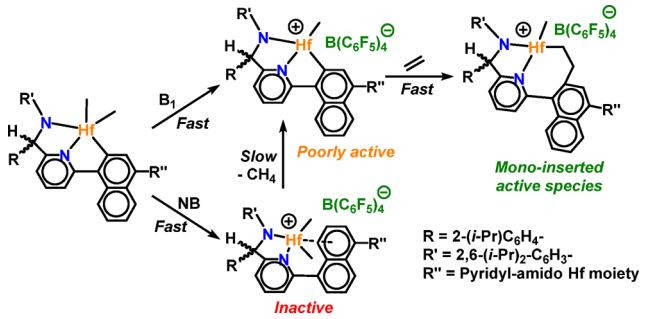

activation with Brønsted acids such as NB leads to selective protonolysis of the Hf−C_{naph} σ- bond, affording an inactive monocationic dimethyl complex stabilized by coordination of the aryl π-system. The latter may undergo aryl remetalation with elimination of CH_4 and subsequent olefin insertion, ultimately affording the active species. However, this process is slow, resulting in long catalytic induction periods (Scheme 5, bottom). From these considerations, the following order of activity is expected for the cationic species generated by activating bimetallic precatalysts **3** and **4** with varying amounts of B_1 and NB: **9** > **6** ≈ **7** ≈ **8** > **5**.

Experimental activity data for both ethylene polymerization and ethylene/1-octene copolymerization are in excellent agreement with the order reported above. Nevertheless, clear indications of cooperativity are found in the significantly enhanced M_w of both polyethylene (5.7 times) and ethylene/1-octene (2.4 times) copolymers as well as the greater incorporation of 1-octene (1.9 times) achieved by **3** when activated by B_1. The observed cooperative enchainment effects involving the two Hf centers in the present systems are not straightforwardly explained. In other bimetallic systems,[2] cooperative effects roughly scale with the accessible M···M distance and may be associated with, in addition to the monomer π-olefin binding, weak secondary interactions between weakly basic monomer substituents (e.g., C−H, Ph) and the second M center (e.g., Scheme 6A).[2a,4a,6] These interactions appear to play a significant role in modifying the enchainment and chain-transfer kinetics.[6]

Scheme 6[a]

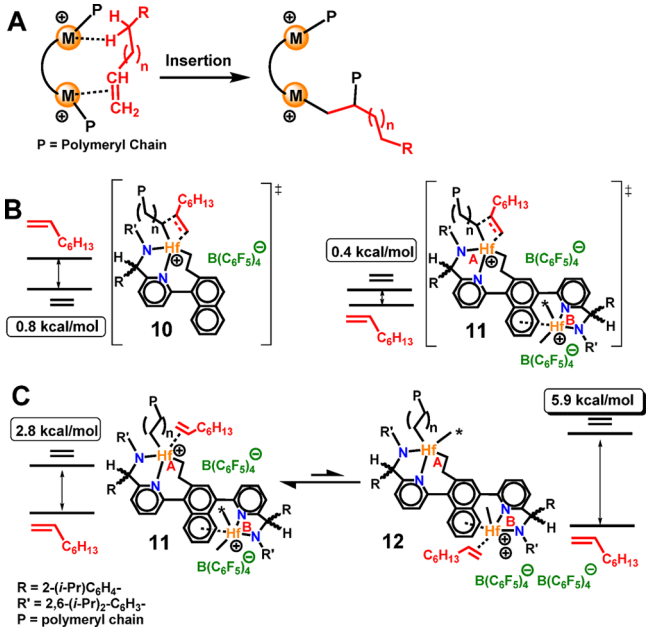

[a](A) Possible mechanistic scenario for enhanced α-olefin enchainment in ethylene-co-α-olefin polymerizations mediated by bimetallic catalysts. (B) Proposed olefin activation/insertion transition states at the Hf centers of activated monometallic species **1** and bimetallic species **11**. (C) Proposed olefin binding equilibrium in complexes formed from bimetallic catalysts **6** and **7**.

The present DFT analysis indicates that in catalysts **6** and **7**, Hf_B lies close enough to Hf_A (Hf_A···Hf_B ranges from 3.20 to 6.55 Å) that 1-octene might π-bond to the Hf_A center while engaging in a −CH_x···M agostic interaction with the Hf_B center, thereby enhancing α-olefin enchainment selectivity. However, alternative scenarios are a priori possible. The simplest is to consider that the Hf_B-moiety may indirectly modify the relative ethylene and 1-octene insertion energy barrier at the active Hf_A center, serving as unusual naphthyl-Hf_A substituent. The present DFT calculations[40] show that the ethylene insertion transition state at the Hf^+ site of activated monometallic catalyst **10** is 0.8 kcal/mol less demanding than that of 1-octene. In contrast, ethylene insertion is 0.4 kcal/mol more demanding at the Hf_A^+ center in the case of the activated bimetallic catalyst **11** (Scheme 6B). Such a slight difference may contribute to the enhanced 1-octene selectivity in the case of the bimetallic

DOI: 10.1021/acscatal.5b00788
ACS Catal. 2015, 5, 5272−5282

catalysts. Moreover, the bulkier naphthyl-Hf_A environment may also modify the catalyst/cocatalyst ion pairing and consequently alter the polymerization properties of the bimetallic catalysts **11**.[41]

A third plausible scenario, based on the fast CH_3 group exchange observed by VT ^{1}H ROESY NMR in **6**, is that at any given time in the catalytic cycle, the mono olefin-uptake bimetallic catalyst equilibrates between the two limiting structures (**11** and **12**) of Scheme 6C. Although this may appear unusual, dicationic metal centers have been previously proposed for Ti^{2+}[42]and Zr^{2+}[43] and recently isolated and characterized in solution by NMR spectroscopy in the case of Hf complexes.[22c] In particular, reaction of monocationic $\mathbf{1}^+B(C_6F_5)_4^-$ with 1 equiv of $HNMe_2Ph^+B(C_6F_5)_4^-$ yields $\mathbf{1}^{2+}[B(C_6F_5)_4^-]_2$.[22c] The relative binding energies of ethylene and 1-octene have been computed for the Hf_A^+ site in **11** and for the Hf_B^{2+} site in **12**. Interestingly, we find that 1-octene coordination to Hf_B^{2+} in **12** lies 5.9 kcal/mol below ethylene coordination, whereas this difference is only 2.8 kcal/mol for olefin binding to the Hf_A^+ center of **11**. This result suggests that **12** may be an intermediate along the polymerization pathway, possibly explaining the greater 1-octene content in the copolymers produced by the present bimetallic catalysts. In this scenario, the Hf_B^{2+} center in **12** is essentially inactive and provides only a lower energy pathway for 1-octene uptake. Once bound to the bimetallic catalyst, the olefin can be easily transferred from one Hf site to the other in concert with alkyl migration, hence equilibrating **11** and **12** (Scheme 6C).[44]

Aside from its origin, the pivotal role played by the close proximity/interplay of the two Hf centers is striking when comparing the polymerization properties of activated precatalysts **3** and **4**. Activation of **4** with 1 or 2 equiv of B_1 produces ion pairs **8** or **9**, respectively (Scheme 4). Both **8** and **9** feature the required Hf−C_{naph} σ-bond(s) amenable to initial ethylene insertion into the Hf−C_{naph} bond and, consequently, are immediately active catalysts (Table 1, entries 4 and 5; Table 2, entries 6 and 7). Note, however, that both produce polymers and copolymers similar to those obtained with monometallic precatalyst **1** (compare entries 1, 2, 4, and 5 in Table 1; entries 1, 3, 6, and 7 in Table 2), despite their bimetallic nature. This lack of enchainment cooperativity is attributable to the larger and fixed $Hf_A\cdots Hf_B$ distance in **9** (7.48 Å, from the DFT optimized structure) vs access to a smaller and flexible $Hf_A\cdots Hf_B$ distance in **6**, 3.20 Å-6.55 Å, from the DFT optimized structures.

3.1. Mechanistic Synopsis. In formulating a concluding cooperativity scenario which encompasses all of the present observations, it is useful to summarize the results:

i. The Hf···Hf distances in bimetallic precatalysts **3** and **4** are 6.16 and 8.06 Å, respectively. Activation with 2 equiv of B_1 generates active species **6** and **9**. DFT computation places the Hf···Hf distance in **6** at 3.20−6.55 Å as a result of the conformationally flexible structure. In contrast, the Hf···Hf distance in **9** is longer (8.06 Å) and conformationally rigid.

ii. NMR studies indicate that, in contrast to monometallic **1**, activation of **3** with NB proceeds by selective and consecutive protonolysis of Hf−CH_3 moieties instead of Hf−C_{naph} protonolysis, as observed for **1**. Consequently, the resulting bimetallic complexes are immediately active for catalytic turnover, whereas the monometallic analogue requires a prolonged induction period.

iii. In comparison with monometallic precatalyst **1** activated with 1 equiv of B_1, bimetallic precatalyst **3** activated with 2 equiv of B_1 (active species **6**) yields polyethylene with 5.7 times higher M_w and poly(ethylene-*co*-1-octene) with 1.9 times greater 1-octene enchainment densities.

iv. In contrast to the above results, bimetallic precatalyst **4** activated with 2 equiv of B_1 (active species **9**) exhibits catalytic behavior (polymer M_w and 1-octene incorporation) similar to that of monometallic precatalyst **1** activated with 1 equiv of B_1.

v. Bimetallic precatalyst **3** activated with 1 equiv of B_1 (active species **5**) exhibits sluggish catalytic behavior and negligible polyethylene M_w enhancement versus monometallic precatalyst **1** activated with 1 equiv of B_1.

vi. In contrast to the above results, bimetallic precatalyst **4** activated with 1 equiv of B_1 (active species **8**) exhibits catalytic behavior (polymer M_w and 1-octene incorporation) similar to that of monometallic precatalyst **1** activated with 1 equiv of B_1.

vii. Although active species **5** and **6** have similar steric characteristics around the Hf centers, ethylene polymerization by **6** gives higher M_w polymer than mononuclear **1**, whereas **5** gives polymer with M_w similar to that of monometallic precatalyst **1** activated with 1 equiv of B_1.

viii. Fast methyl exchange is observed in **5** and **6** by NMR, indicating that alkyl groups can rapidly and reversibly transfer between the Hf_A and Hf_B catalytic centers, as also suggested by DFT calculations.

Scheme 6 presents a qualitative scenario for the reader that we feel best portrays the present observations, paralleling a picture that has evolved for other bimetallic polymerization systems.

4. CONCLUSIONS

This investigation reports the synthesis and characterization of a series of bimetallic pyridylamido Hf catalysts. Bimetallic complexes **3** and **4**, with varied solid state spatial conformations and Hf···Hf distances exhibit distinctive and opposite catalytic behavior. The shorter and more flexible Hf···Hf distance in the **3**-derived active species affords product polymers with higher M_w and copolymers with enhanced 1-octene incorporation vs those obtained with monometallic analogue **1**. In contrast, the **4**-derived active species having a larger and fixed Hf···Hf distance produces polymers and copolymers similar to those obtained with monometallic catalyst **1**. It is noteworthy that the observation of very rapid exchange of alkyl and by extension, polymeryl, moieties between two Hf centers in **6** suggests that the Hf···Hf proximity may render intramolecular chain shuttling possible, even in the absence of a chain shuttling agent.[45] This possibility is currently under investigation.

■ ASSOCIATED CONTENT

Supporting Information

The Supporting Information is available free of charge on the ACS Publications website at DOI: 10.1021/acscatal.5b00788.

Details of ligand and catalyst synthesis/characterization, polymerization experiments, polymer characterization, 1D and 2D NMR spectra, and DFT calculations (PDF)
Crystallographic details (CIF, CIF, CIF, CIF)

DOI: 10.1021/acscatal.5b00788
ACS Catal. 2015, 5, 5272−5282

AUTHOR INFORMATION

Corresponding Authors

*E-mail: cristiano.zuccaccia@unipg.it.
*E-mail: alceo.macchioni@unipg.it.
*E-mail: m-delferro@northwestern.edu.
*E-mail: t-marks@northwestern.edu.

Notes

The authors declare no competing financial interest.

ACKNOWLEDGMENTS

Financial support by DOE (Grant 86ER13511; heterogeneous and solution phase olefin polymerization) and NSF (Grant CHE-1213235) is gratefully acknowledged. Purchase of the NMR instrumentation at IMSERC was supported by NSF (CHE-1048773). Diffractometry experiments were conducted at IMSERC on Bruker Kappa APEX II instruments purchased with assistance from the State of Illinois and Northwestern University. Computational resources supporting this work were provided by the Northwestern University Quest High Performance Computing cluster (M.D.). A.M. and C.Z. thank CIRCC (Interuniversity Consortium for Chemical Reactivity and Catalysis) and UNIVATION for financial support. Y.G. thanks the Shanghai Institute of Organic Chemistry (SIOC, CAS) for a Postdoctoral Fellowship. We also thank Albemarle Corp. for a generous gift of triphenylcarbenium tetrakis(pentafluorophenyl)borate, $Ph_3C^+B(C_6F_5)_4^-$ and Boulder Scientific Co. for generous gifts of dimethylanilinium tetrakis(pentafluorophenyl) borate; $PhNMe_2H^+B(C_6F_5)_4^-$; and tetrakis(dimethylamido) hafnium, $Hf(NMe_2)_4$.

REFERENCES

(1) (a) Mitić, N.; Smith, S. J.; Neves, A.; Guddat, L. W.; Gahan, L. R.; Schenk, G. *Chem. Rev.* **2006**, *106*, 3338−3363. (b) Collman, J. P.; Boulatov, R.; Sunderland, C. J.; Fu, L. *Chem. Rev.* **2004**, *104*, 561−588. (c) Steinhagen, H.; Helmchen, G. *Angew. Chem., Int. Ed. Engl.* **1996**, *35*, 2339−2342. (d) Sträter, N.; Lipscomb, W. N.; Klabunde, T.; Krebs, B. *Angew. Chem., Int. Ed. Engl.* **1996**, *35*, 2024−2055.

(2) (a) McInnis, J. P.; Delferro, M.; Marks, T. J. *Acc. Chem. Res.* **2014**, *47*, 2545−2557. (b) Delferro, M.; Marks, T. J. *Chem. Rev.* **2011**, *111*, 2450−2485.

(3) (a) Guo, N.; Stern, C. L.; Marks, T. J. *J. Am. Chem. Soc.* **2008**, *130*, 2246−2261. (b) Li, H.; Li, L.; Schwartz, D. J.; Metz, M. V.; Marks, T. J.; Liable-Sands, L.; Rheingold, A. L. *J. Am. Chem. Soc.* **2005**, *127*, 14756−14768. (c) Guo, N.; Li, L.; Marks, T. J. *J. Am. Chem. Soc.* **2004**, *126*, 6542−6543. (d) Li, H.; Li, L.; Marks, T. J.; Liable-Sands, L.; Rheingold, A. L. *J. Am. Chem. Soc.* **2003**, *125*, 10788−10789.

(4) (a) Motta, A.; Fragala, I. L.; Marks, T. J. *J. Am. Chem. Soc.* **2009**, *131*, 3974−3984. (b) Li, H.; Li, L.; Marks, T. J. *Angew. Chem., Int. Ed.* **2004**, *43*, 4937−4940. (c) Li, L.; Metz, M. V.; Li, H.; Chen, M.-C.; Marks, T. J.; Liable-Sands, L.; Rheingold, A. L. *J. Am. Chem. Soc.* **2002**, *124*, 12725−12741.

(5) Wang, J.; Li, H.; Guo, N.; Li, L.; Stern, C. L.; Marks, T. J. *Organometallics* **2004**, *23*, 5112−5114.

(6) (a) Liu, S.; Motta, A.; Mouat, A. R.; Delferro, M.; Marks, T. J. *J. Am. Chem. Soc.* **2014**, *136*, 10460−10469. (b) Liu, S.; Motta, A.; Delferro, M.; Marks, T. J. *J. Am. Chem. Soc.* **2013**, *135*, 8830−8833.

(7) (a) Salata, M. R.; Marks, T. J. *Macromolecules* **2009**, *42*, 1920−1933. (b) Salata, M. R.; Marks, T. J. *J. Am. Chem. Soc.* **2008**, *130*, 12−13.

(8) (a) Radlauer, M. R.; Buckley, A. K.; Henling, L. M.; Agapie, T. *J. Am. Chem. Soc.* **2013**, *135*, 3784−3787. (b) Radlauer, M. R.; Day, M. W.; Agapie, T. *J. Am. Chem. Soc.* **2012**, *134*, 1478−1481.

(9) (a) Weberski, M. P.; Chen, C.; Delferro, M.; Marks, T. J. *Chem. - Eur. J.* **2012**, *18*, 10715−10732. (b) Rodriguez, B. A.; Delferro, M.; Marks, T. J. *Organometallics* **2008**, *27*, 2166−2168.

(10) (a) Wei, J.; Hwang, W.; Zhang, W.; Sita, L. R. *J. Am. Chem. Soc.* **2013**, *135*, 2132−2135. (b) Zhang, W.; Wei, J.; Sita, L. R. *Macromolecules* **2008**, *41*, 7829−7833. (c) Zhang, W.; Sita, L. R. *Adv. Synth. Catal.* **2008**, *350*, 439−447. (d) Diamond, G. M.; Chernega, A. N.; Mountford, P.; Green, M. L. H. *J. Chem. Soc., Dalton Trans.* **1996**, 921−938.

(11) Resconi, L.; Cavallo, L.; Fait, A.; Piemontesi, F. *Chem. Rev.* **2000**, *100*, 1253−1346.

(12) (a) Klosin, J.; Fontaine, P. P.; Figueroa, R. *Acc. Chem. Res.* **2015**, *48*, 2004−2016. (b) Baier, M. C.; Zuideveld, M. A.; Mecking, S. *Angew. Chem., Int. Ed.* **2014**, *53*, 9722−9744. (c) Makio, H.; Terao, H.; Iwashita, A.; Fujita, T. *Chem. Rev.* **2011**, *111*, 2363−2449. (d) Gibson, V. C.; Spitzmesser, S. K. *Chem. Rev.* **2003**, *103*, 283−316. (e) Britovsek, G. J. P.; Gibson, V. C.; Wass, D. F. *Angew. Chem., Int. Ed.* **1999**, *38*, 428−447.

(13) (a) Wei, J.; Zhang, W.; Wickham, R.; Sita, L. R. *Angew. Chem., Int. Ed.* **2010**, *49*, 9140−9144. (b) Wei, J.; Zhang, W.; Sita, L. R. *Angew. Chem., Int. Ed.* **2010**, *49*, 1768−1772. S1768/1761-S1768/1767 (c) Zhang, W.; Sita, L. R. *J. Am. Chem. Soc.* **2008**, *130*, 442−443.

(14) (a) Tsurugi, H.; Ohnishi, R.; Kaneko, H.; Panda, T. K.; Mashima, K. *Organometallics* **2009**, *28*, 680−687. (b) De Waele, P.; Jazdzewski, B. A.; Klosin, J.; Murray, R. E.; Theriault, C. N.; Vosejpka, P. C.; Petersen, J. L. *Organometallics* **2007**, *26*, 3896−3899.

(15) (a) Fontaine, P. P.; Figueroa, R.; McCann, S. D.; Mort, D.; Klosin, J. *Organometallics* **2013**, *32*, 2963−2972. (b) Figueroa, R.; Froese, R. D.; He, Y.; Klosin, J.; Theriault, C. N.; Abboud, K. A. *Organometallics* **2011**, *30*, 1695−1709.

(16) Fontaine, P. P.; Klosin, J.; McDougal, N. T. *Organometallics* **2012**, *31*, 6244−6251.

(17) Szuromi, E.; Klosin, J.; Abboud, K. A. *Organometallics* **2011**, *30*, 4589−4597.

(18) (a) Takii, Y.; Inagaki, A.; Nomura, K. *Dalton Trans.* **2013**, *42*, 11632−11639. (b) Nifant'ev, I. E.; Ivchenko, P. V.; Bagrov, V. V.; Nagy, S. M.; Winslow, L. N.; Merrick-Mack, J. A.; Mihan, S.; Churakov, A. V. *Dalton Trans.* **2013**, *42*, 1501−1511. (c) Li, G.; Lamberti, M.; Roviello, G.; Pellecchia, C. *Organometallics* **2012**, *31*, 6772−6778. (d) Yuan, S.; Wei, X.; Tong, H.; Zhang, L.; Liu, D.; Sun, W.-H. *Organometallics* **2010**, *29*, 2085−2092. (e) Marquet, N.; Kirillov, E.; Roisnel, T.; Razavi, A.; Carpentier, J.-F. *Organometallics* **2009**, *28*, 606−620. (f) Golisz, S. R.; Bercaw, J. E. *Macromolecules* **2009**, *42*, 8751−8762. (g) Janas, Z.; Godbole, D.; Nerkowski, T.; Szczegot, K. *Dalton Trans.* **2009**, 8846−8853. (h) Lamberti, M.; Mazzeo, M.; Pellecchia, C. *Dalton Trans.* **2009**, 8831−8837. (i) Gong, S.; Ma, H.; Huang, J. *Dalton Trans.* **2009**, 8237−8247. (j) Niemeyer, J.; Kehr, G.; Froehlich, R.; Erker, G. *Dalton Trans.* **2009**, 3731−3741. (k) Long, R. J.; Gibson, V. C.; White, A. J. P. *Organometallics* **2008**, *27*, 235−245. (l) Ramos, C.; Royo, P.; Lanfranchi, M.; Pellinghelli, M. A.; Tiripicchio, A. *Organometallics* **2007**, *26*, 445−454.

(19) Fan, L.; Harrison, D.; Woo, T. K.; Ziegler, T. *Organometallics* **1995**, *14*, 2018−2026.

(20) (a) Busico, V.; Cipullo, R.; Pellecchia, R.; Talarico, G.; Razavi, A. *Macromolecules* **2009**, *42*, 1789−1791. (b) Bryliakov, K. P.; Talsi, E. P.; Voskoboynikov, A. Z.; Lancaster, S. J.; Bochmann, M. *Organometallics* **2008**, *27*, 6333−6342.

(21) (a) Boussie, T. R.; Diamond, G. M.; Goh, C.; Hall, K. A.; LaPointe, A. M.; Leclerc, M.; Lund, C.; Murphy, V.; Shoemaker, J. A. W.; Tracht, U.; Turner, H.; Zhang, J.; Uno, T.; Rosen, R. K.; Stevens, J. C. *J. Am. Chem. Soc.* **2003**, *125*, 4306−4317. (b) Boussie, T. R.; Diamond, G. M.; Goh, C.; Hall, K. A.; LaPointe, A. M.; Leclerc, M. K.; Murphy, V.; Shoemaker, J. A. W.; Turner, H.; Rosen, R. K.; Stevens, J. C.; Alfano, F.; Busico, V.; Cipullo, R.; Talarico, G. *Angew. Chem., Int. Ed.* **2006**, *45*, 3278−3283.

(22) (a) Busico, V.; Cipullo, R.; Pellecchia, R.; Rongo, L.; Talarico, G.; Macchioni, A.; Zuccaccia, C.; Froese, R. D. J.; Hustad, P. D. *Macromolecules* **2009**, *42*, 4369−4373. (b) Zuccaccia, C.; Busico, V.; Cipullo, R.; Talarico, G.; Froese, R. D. J.; Vosejpka, P. C.; Hustad, P. D.; Macchioni, A. *Organometallics* **2009**, *28*, 5445−5458. (c) Zuccaccia, C.; Macchioni, A.; Busico, V.; Cipullo, R.; Talarico, G.; Alfano, F.; Boone, H. W.; Frazier, K. A.; Hustad, P. D.; Stevens, J. C.; Vosejpka, P.

DOI: 10.1021/acscatal.5b00788
ACS Catal. 2015, 5, 5272−5282

C.; Abboud, K. A. *J. Am. Chem. Soc.* **2008**, *130*, 10354−10368. (d) Froese, R. D. J.; Hustad, P. D.; Kuhlman, R. L.; Wenzel, T. T. *J. Am. Chem. Soc.* **2007**, *129*, 7831−7840. (e) Boussie, T. R.; Diamond, G. M.; Goh, C.; Hall, K. A.; LaPointe, A. M.; Leclerc, M. K.; Murphy, V.; Shoemaker, J. A. W.; Turner, H.; Rosen, R. K.; Stevens, J. C.; Alfano, F.; Busico, V.; Cipullo, R.; Talarico, G. *Angew. Chem., Int. Ed.* **2006**, *45*, 3278−3283. (f) Rocchigiani, L.; Busico, V.; Pastore, A.; Talarico, G.; Macchioni, A. *Angew. Chem., Int. Ed.* **2014**, *53*, 2157−2161.

(23) (a) Yoder, J. C.; Bercaw, J. E. *J. Am. Chem. Soc.* **2002**, *124*, 2548−2555. (b) Busico, V.; Cipullo, R.; Caporaso, L.; Angelini, G.; Segre, A. L. *J. Mol. Catal. A: Chem.* **1998**, *128*, 53−64. (c) Leclerc, M. K.; Brintzinger, H. H. *J. Am. Chem. Soc.* **1995**, *117*, 1651−1652.

(24) Arriola, D. J.; Carnahan, E. M.; Hustad, P. D.; Kuhlman, R. L.; Wenzel, T. T. *Science* **2006**, *312*, 714−719.

(25) (a) Kuhlman, R. L.; Klosin, J. *Macromolecules* **2010**, *43*, 7903−7904. (b) Hustad, P. D.; Kuhlman, R. L.; Arriola, D. J.; Carnahan, E. M.; Wenzel, T. T. *Macromolecules* **2007**, *40*, 7061−7064.

(26) Frazier, K. A.; Froese, R. D.; He, Y.; Klosin, J.; Theriault, C. N.; Vosejpka, P. C.; Zhou, Z.; Abboud, K. A. *Organometallics* **2011**, *30*, 3318−3329.

(27) Bimetallic Hf(IV) amido complex **2** was synthesized via protodeamination of excess of $Hf(NMe_2)_4$ with L^2 in refluxing toluene with continuous removal of the volatile $HNMe_2$ byproduct until disappearance of the N−H peak as tracked by ^1H NMR (Scheme 2). Single crystals of **2** suitable for X-ray diffraction studies were grown from concentrated toluene solution.

(28) Li, G.; Zuccaccia, C.; Tedesco, C.; D'Auria, I.; Macchioni, A.; Pellecchia, C. *Chem. - Eur. J.* **2014**, *20*, 232−244.

(29) (a) Stephenson, C. J.; McInnis, J. P.; Chen, C.; Weberski, M. P.; Motta, A.; Delferro, M.; Marks, T. J. *ACS Catal.* **2014**, *4*, 999−1003. (b) Weberski, M. P.; Chen, C.; Delferro, M.; Zuccaccia, C.; Macchioni, A.; Marks, T. J. *Organometallics* **2012**, *31*, 3773−3789.

(30) (a) Kaminsky, W. *Macromolecules* **2012**, *45*, 3289−3297. (b) Bochmann, M. *Organometallics* **2010**, *29*, 4711−4740. (c) Chen, E. Y.-X.; Marks, T. J. *Chem. Rev.* **2000**, *100*, 1391−1434.

(31) Möhring, P. C.; Coville, N. J. *Coord. Chem. Rev.* **2006**, *250*, 18−35.

(32) NMR activation study of **4** + 1 equiv of NB indicates selective formation of polymerization inactive complex **5**; however, in the presence of a slight excess of NB, a small amount of highly active catalyst **7** can be formed, which likely accounts for the observed polymerization properties.

(33) (a) McDaniel, M. P.; Schwerdtfeger, E. D.; Jensen, M. D. *J. Catal.* **2014**, *314*, 109−116. (b) Nikolaeva, M. I.; Matsko, M. A.; Mikenas, T. B.; Echevskaya, L. G.; Zakharov, V. A. *J. Appl. Polym. Sci.* **2012**, *125*, 2034−2041. (c) Laine, A.; Linnolahti, M.; Pakkanen, T. A.; Severn, J. R.; Kokko, E.; Pakkanen, A. *Organometallics* **2011**, *30*, 1350−1358. (d) Awudza, J. A. M.; Tait, P. J. T. *J. Polym. Sci., Part A: Polym. Chem.* **2008**, *46*, 267−277. (e) Stadler, F. J.; Piel, C.; Klimke, K.; Kaschta, J.; Parkinson, M.; Wilhelm, M.; Kaminsky, W.; Muenstedt, H. *Macromolecules* **2006**, *39*, 1474−1482. (f) Smit, M.; Zheng, X.; Bruell, R.; Loos, J.; Chadwick, J. C.; Koning, C. E. *J. Polym. Sci., Part A: Polym. Chem.* **2006**, *44*, 2883−2890. (g) Koivumaki, J.; Seppala, J. V. *Macromolecules* **1993**, *26*, 5535−5538.

(34) Randall, J. C. *J. Macromol. Sci., Polym. Rev.* **1989**, *29*, 201−317.

(35) (a) Galland, G. B.; Quijada, P.; Mauler, R. S.; de Menezes, S. C. *Macromol. Rapid Commun.* **1996**, *17*, 607−613. (b) Uozumi, T.; Soga, K. *Makromol. Chem.* **1992**, *193*, 823−831.

(36) (a) Kiesewetter, E. T.; Waymouth, R. M. *Macromolecules* **2013**, *46*, 2569−2575. (b) Chai, J. F.; Abboud, K. A.; Miller, S. A. *Dalton Trans.* **2013**, *42*, 9139−9147. (c) Stagnaro, P.; Boragno, L.; Losio, S.; Canetti, M.; Alfonso, G. C.; Galimberti, M.; Piemontesi, F.; Sacchi, M. C. *Macromolecules* **2011**, *44*, 3712−3722. (d) Hung, J.; Cole, A. P.; Waymouth, R. M. *Macromolecules* **2003**, *36*, 2454−2463. (e) Galimberti, M.; Piemontesi, F.; Fusco, O.; Camurati, I.; Destro, M. *Macromolecules* **1998**, *31*, 3409−3416.

(37) NMR peak assignment of relevant resonances and determination of the three-dimensional structure in solution for some of the complexes were carried out crossing the information from 1D- and 2D- homo- and heteronuclear NMR experiments. Because of severe overlapping, not all the resonances could be assigned. Dicationic ion pairs, obtained using 2 equiv of activators, were poorly soluble and separated from the benzene or toluene solutions as deep orange-red oils. In those cases, the oil was separated, and subsequent NMR characterization was carried out by redissolving it in chlorobenzene-d_5. The ^{13}C and ^{19}F NMR resonances of the $B(C_6F_5)_4^-$ anion are unexceptional and are not commented.

(38) Ethylene/1-octene copolymerization using catalyst **3** with 3.4 equiv of B_1 shows results (4032 (kg of polymer) (mol of Hf)$^{-1}$ h^{-1} atm^{-1}, 1-octene incorporation ratio 18.9%, M_w is 401 kg/mol) similar to the copolymerization with 2.4 equiv, suggesting no further methyl abstraction from the Hf_B.

(39) (a) Luconi, L.; Klosin, J.; Smith, A. J.; Germain, S.; Schulz, E.; Hannedouche, J.; Giambastiani, G. *Dalton Trans.* **2013**, *42*, 16056−16065. (b) Domski, G. J.; Edson, J. B.; Keresztes, I.; Lobkovsky, E. B.; Coates, G. W. *Chem. Commun.* **2008**, 6137−6139.

(40) DFT calculations were carried out on the active species with an ethylene unit inserted between the Hf center and the naphthyl moiety

(41) (a) Roberts, J. A. S.; Chen, M.-C.; Seyam, A. M.; Li, L.; Zuccaccia, C.; Stahl, N. G.; Marks, T. J. *J. Am. Chem. Soc.* **2007**, *129*, 12713−12733. (b) Chen, M. C.; Roberts, J. A. S.; Seyam, A. M.; Li, L. T.; Zuccaccia, C.; Stahl, N. G.; Marks, T. J. *Organometallics* **2006**, *25*, 2833−2850. (c) Zuccaccia, C.; Stahl, N. G.; Macchioni, A.; Chen, M.-C.; Roberts, J. A.; Marks, T. J. *J. Am. Chem. Soc.* **2004**, *126*, 1448−1464. (d) Chen, M.-C.; Roberts, J. A. S.; Marks, T. J. *J. Am. Chem. Soc.* **2004**, *126*, 4605−4625.

(42) (a) Chen, E. Y. X.; Kruper, W. J.; Roof, G.; Wilson, D. R. *J. Am. Chem. Soc.* **2001**, *123*, 745−746. (b) Guérin, F.; Stewart, J. C.; Beddie, C.; Stephan, D. W. *Organometallics* **2000**, *19*, 2994−3000.

(43) (a) Stahl, N. G.; Salata, M. R.; Marks, T. J. *J. Am. Chem. Soc.* **2005**, *127*, 10898−10909. (b) Green, M. L. H.; Saßmannshausen, J. *Chem. Commun.* **1999**, 115−116. (c) Bosch, B. E.; Erker, G.; Fröhlich, R.; Meyer, O. *Organometallics* **1997**, *16*, 5449−5456.

(44) The difference in energy between structures **11** and **12** is 13.1 kcal/mol in the case of ethylene and 10.0 kcal/mol for the 1-octene. These values are probably overstimed because neither counteranion nor solvent is taken into account (polar solvent, in particular, reduces the destabilization as a result of charge concentration). We have neglected the counteranion and solvent because of the size of the system. Obviously, this approximation does not affect the energy comaprison between ethylene and 1-octene uptake at catalyst species **11** or **12**.

(45) (a) Valente, A.; Mortreux, A.; Visseaux, M.; Zinck, P. *Chem. Rev.* **2013**, *113*, 3836−3857. (b) Sita, L. R. *Angew. Chem., Int. Ed.* **2009**, *48*, 2464−2472. (c) Kempe, R. *Chem. - Eur. J.* **2007**, *13*, 2764−2773. (d) van Meurs, M.; Britovsek, G. J. P.; Gibson, V. C.; Cohen, S. A. *J. Am. Chem. Soc.* **2005**, *127*, 9913−9923.

DOI: 10.1021/acscatal.5b00788
ACS Catal. 2015, 5, 5272−5282